Overview of ASDEX Upgrade Results

O. Gruber, H.-S. Bosch, S. Günter, A. Herrmann, A. Kallenbach, M. Kaufmann, K. Krieger, K. Lackner, V. Mertens, R. Neu, F. Ryter, J. Schweinzer, A. Stäbler, W. Suttrop, R. Wolf, K. Asmussen, A. Bard, G. Becker, K. Behler, K. Behringer, A. Bergmann, M. Bessenrodt-Weberpals, K. Borrass, B. Braams[1], M. Brambilla, R. Brandenburg[2], F. Braun, H. Brinkschulte, R. Brückner, B. Brüsehaber, K. Büchl, A. Buhler, A. Carlson, H. Callaghan[3], D. Coster, L. Cupido[4], S. de Peña Hempel, C. Dorn, R. Drube, R. Dux, S. Egorov[5], W. Engelhardt, H.-U. Fahrbach, U. Fantz[6], H.-U. Feist, P. Franzen, J. C. Fuchs, G. Fussmann, J. Gafert, G. Gantenbein[7], O. Gehre, A. Geier, J. Gernhardt, E. Gubanka, A. Gude, G. Haas, K. Hallatschek, J. Hartmann, B. Heinemann, G. Herppich, W. Herrmann, F. Hofmeister, E. Holzhauer[7], D. Jacobi, M. Kakoulidis[8], N. Karakatsanis[8], O. Kardaun, A. Khutoretski[9], H. Kollotzek, S. Kötterl, W. Kraus, B. Kurzan, G. Kyriakakis[8], P. T. Lang, R. S. Lang, M. Laux, L. Lengyel, F. Leuterer, A. Lorenz, H. Maier, M. Manso[4], M. Maraschek, M. Markoulaki[8], K.-F. Mast, P. McCarthy[3], D. Meisel, H. Meister, R. Merkel, J. P. Meskat[7], H. W. Müller, M. Münich, H. Murmann, B. Napiontek, G. Neu, J. Neuhauser, M. Niethammer, J.-M. Noterdaeme, G. Pautasso, A. G. Peeters, G. Pereverzev, G. Raupp, K. Reinmüller, R. Riedl, V. Rohde, H. Röhr, J. Roth, H. Salzmann, W. Sandmann, H.-B. Schilling, D. Schlögl, K. Schmidtmann, H. Schneider, R. Schneider, W. Schneider, G. Schramm, S. Schweizer, R. R. Schwörer, B. D. Scott, U. Seidel, F. Serra[4], S. Sesnic, C. Sihler, A. Silva[4], E. Speth, K.-H. Steuer, J. Stober, B. Streibl, A. Thoma, W. Treutterer, M. Troppmann, N. Tsois[8], W. Ullrich, M. Ulrich, P. Varela[4], H. Verbeek, O. Vollmer, H. Wedler, M. Weinlich, U. Wenzel, F. Wesner, R. Wunderlich, N. Xantopoulos[8], Q. Yu[10], D. Zasche, T. Zehetbauer, H.-P. Zehrfeld, H. Zohm[7] and M. Zouhar.

Max-Planck-Institut für Plasmaphysik, EURATOM-IPP Association,
Garching and Berlin, Germany

[1] New York University, NJ, USA
[2] Technical University of Vienna, Austria
[3] University College Cork, Republic of Ireland
[4] Centro de Fusão Nuclear, Lisbon, Portugal
[5] Efremov Institute, St. Petersburg, Russia
[6] University of Augsburg, Germany
[7] IPF, University of Stuttgart, Germany
[8] NSCR Demokritos, Athens, Greece
[9] Kurchatov Institute, Moscow, Russia
[10] Academia Sinica, Hefei, China

Abstract

The closed ASDEX Upgrade divertor II “Lyra” is capable to handle heating powers up to 20 MW or P/R of 12 MW/m due to a reduction of maximum heat flux to the target plates by more than a factor of two compared to the open divertor I. This reduction is caused by high radiative losses from carbon and hydrogen inside the divertor region and is in agreement with B2-Eirene modelling predictions.

At medium densities in the H-mode the type-I ELM behaviour shows no dependence from the heating method (NBI, ICRH). ASDEX Upgrade-JET dimensionless identity experiments showed compatibility of the L-H transition with core physics constraints, while in the H-mode confinement inconsistencies with the invariance principle were established.

At high densities close to the Greenwald density the MHD limited edge pressures, influence of divertor detachment on seperatrix parameters and increasing edge transport lead to limited edge densities and finally temperatures below the critical edge temperatures for H-mode. This results in a drastically increase of the H-mode threshold power and an upper H-mode density limit with gas-puff refuelling. The

H-mode confinement degradation approaching this density limit is caused by the ballooning mode limited edge pressures and "stiff" temperature profiles relating core and edge temperatures. Repetitive high-field side pellet injection allows for H-mode operation well above the Greenwald density, and moreover higher confinement than with gas fuelling is found up to the highest densities.

Neoclassical tearing modes limit the achievable β depending on the collisionality at the resonant surface. In agreement with the polarization current model the onset β is found to be proportional to the ion gyro-radius in the collisionless regime, while higher collisionalities are stabilizing. The fractional energy loss connected with saturated modes at high pressures is about 25 %. Reduction of neoclassical mode amplitude and increase of β has been demonstrated by using phased ECR heating and current drive in the islands O-point.

Advanced tokamak operation with internal transport barriers for both ions and electrons have been achieved with flat shear profiles and $q_0 > 1$ or with reversed shear and $q_{min} > 2$. With flat shear a stationary H-mode scenario was maintained for 40 confinement times and several internal skin times with $\beta_N = 2$ and an $H_{ITER-89P} = 2.4$, where fishbones keep the q_0 at one. β_N is limited by either neoclassical tearing modes in case of flat shear or kink modes with reversed shear.

1. Introduction

The ASDEX Upgrade non-circular tokamak programme has largely been concerned with edge and divertor physics in the high-power H-mode regime with the new Div II divertor configuration, with the aim of identifying and optimizing ways for safe power exhaust and particle control (ash removal). Additionally, during the last few years core physics, confinement and performance related, have played an increasingly important role. Especially edge-core interaction has been the subject of pioneering work in ASDEX Upgrade. The edge operational diagram introduced characterizes different edge operating conditions for L- and H-mode in connection with the ballooning and density limits. MHD stability and β limits as well as the avoidance and mitigation of disruptions have been further main topics. Investigation of scenarios and physics of advanced tokamak plasma concepts has also been started. Alignment of the internal transport barrier with the optimal shear profile and the compatibility of this new idea with stationary operation at high power and, simultaneously, a cold divertor are to be the key elements of this future programme.

Here the similarity of ASDEX Upgrade to ITER in poloidal field coil system and divertor configuration makes it particularly suited to testing control strategies for shape, plasma performance and mode stabilization (e.g. feedback stabilization of neoclassical MHD modes with ECRH/CD). Additionally, the similarity in cross-section ($R/a = 3.3$, $\kappa \leq 1.8$, $\delta \leq 0.2$) to other divertor tokamaks is important in determining size scalings for core and edge physics. This collaborative work, including extrapolation to ITER parameters, has continued with emphasis on the confinement scaling at high densities.

Since the summer of 1997, ASDEX Upgrade has been operated with the new Div II installation, "LYRA", and with a cryompump (100 m^3/s pumping speed), both shown in Fig. 1 together with the previous configuration (Div I).

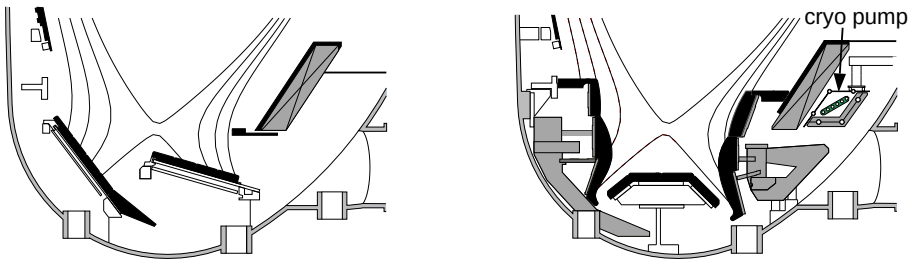

Figure 1: Poloidal cross-section of the original ASDEX Upgrade Divertor I (left) and of the new Divertor II (LYRA, right). The flux surfaces in both figures have a radial separation of 12 mm in the plasma midplane.

While Div I used flat target plates (covered with fine-grain graphite) close to the X-point to benefit from the large flux expansion there, Div II has vertical, lyre-shaped targets to reflect the neutrals created at the target preferentially towards the power-conducting sheath close to the separatrix, and to make the target heat load distribution as homogenous as possible. Details of the design, which is rather similar to the present ITER reference design, are described in [1].

At the same time, the heating systems were substantially upgraded. For neutral beam injection of D^0 at 60 keV, a second injector box was installed, providing a total NBI power of 20 MW in D^0, and 14 MW in H^0. The scaling parameter P/R for divertor discharges now reaches values of about 12 MW/m, roughly a factor of only 3 below the ITER value. This heating power further allows β limit and MHD stability studies with toroidal fields of up to 3 T and extended H-mode studies in hydrogen. The ICRH system was equipped with 3 db couplers [2] to enhance the system efficiency in ELMy plasmas, allowing coupling of the full power of 5.7 MW. The ECRH system now consists of two gyrotrons with a power of 0.8 MW for 2 s, allowing stabilization of neoclassical modes [3,4], and transport studies, as described later. The pellet injection system was modified to allow pellet injection from the high-field side (HFS) now also with a centrifuge [5].

The following sections discuss the main topics of the ASDEX Upgrade experiments, viz. energy and particle exhaust (Sect. 2), confinement (Sect. 3) and H-mode physics (Sect. 4), operation at high density, including high-field-side pellet injection (Sect. 5), characterization and feedback stabilization of neoclassical tearing modes (Sect. 6) and concept improvement with internal transport barriers, demonstrating the possibility of steady state together with an H-mode edge (Sect. 7).

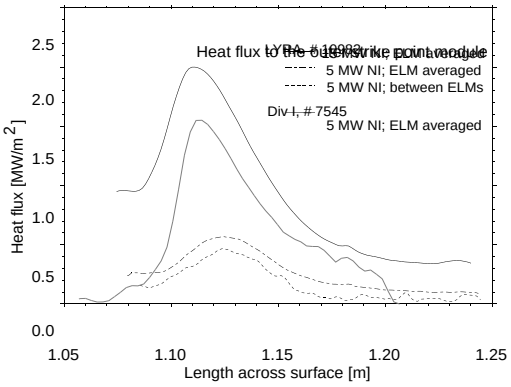

Figure 2: Heat flux to the outer strike point region measured by infrared thermography as comparison for Div I and Div II. In Div II, a heating power of 15 MW leads to a heat flux on the target plate which is similar to that in Div I with only 5 MW of heating power. At the same heating power, the heat flux in Div II is significantly reduced.

2. Energy and particle exhaust

A detailed overview of energy and particle exhaust in Div II is presented in [6]. The LYRA divertor has been very successfully operated, and the maximum heat flux on the target plates has been reduced by a factor of more than 2, compared with Div I (Fig. 2). The maximum heat flux in discharges with input powers of up to 20 MW is below 5 MW/m^2. This reduction of the power flow results from an increased radiative power loss, which is concentrated in the divertor region. With Div II, about 45 % of the input power is radiated below the X-point (75 % total). Most of the divertor radiation is concentrated in a small emission zone along the separatrix, as measured with bolometry during a vertical sweep of the plasma. This was already predicted by modelling with the B2-Eirene code, and the agreement is shown in Fig. 3. There are two pronounced radiation density peaks in both the inner and outer divertor fan with values of up to 15 MW/m^3. The predicted radiation band is clearly seen with a width of a few centimetres and a radiation density of about 3-4 MW/m^3 at the inner divertor. Since there are no suitable lines of sight for the outer divertor yet, the corresponding band cannot be detected there. In the main plasma one finds radiation mainly along the separatrix with radiation densities below 1 MW/m^3.

The enhanced divertor radiation is not caused by a stronger influx of carbon, but is due to an increased combined radiation efficiency of carbon and hydrogen in the divertor plasma. Carbon cools the SOL plasma down to the 5 eV region, where hydrogen losses become significant. This process is based on

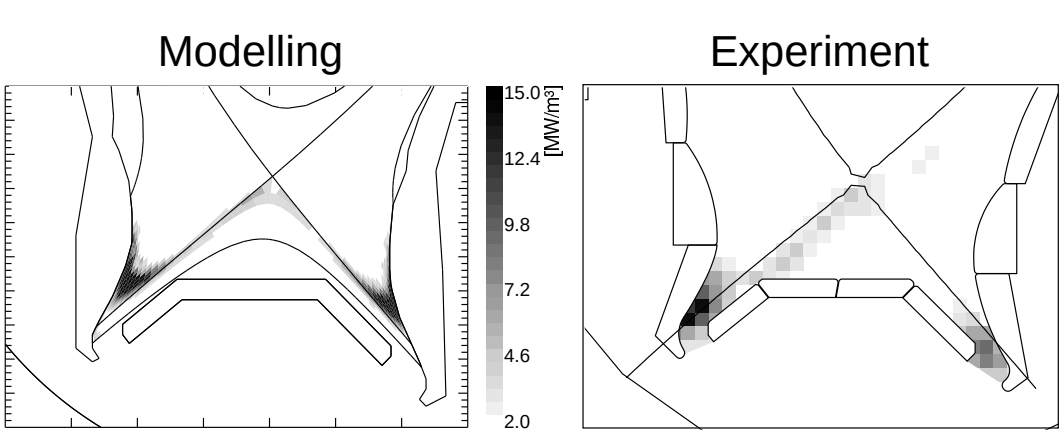

Figure 3: a) (left): B2-Eirene modelling of the radiation distribution predicts radiation bands between the X-point and strike points. b) (right): The reconstructed radiation distribution using virtual lines of sight during vertical shift of the plasma reveals a narrow radiation band between the inner strike point and X-point.

the interplay between the following four effects, as could be partly disentangled by 2D modelling and experimental parameter variations:

- Neutrals are reflected towards the "hot" separatrix region due to the highly inclined target plates.
- The high density and an electron temperature of a few eV allow effective radiation of hydrogen. Carbon produces the necessary pre-cooling of the divertor plasma to make the hydrogenic losses more effective.
- The volume for radiation is increased by broadening of the SOL due to radial transport. This is especially the case for discharges with type-I ELMs, as is found experimentally [7]. Under these conditions ($P_{heat} \geq 2.5$ MW) the boundary is at the ballooning limit, resulting in an increase of $\chi_\perp$ with rising power.

B2-Eirene modelling describes the experimental data if the carbon sputter yield and the perpendicular transport coefficients are properly adapted, and allows an insight into the physical mechanisms responsible for the increase of the divertor radiation [8].

The fact that the fractional radiative loss in the divertor is rather independent of the heating power suggests that self-regulating mechanisms are effective. For relatively cold divertor conditions, the particle flux at the target increases with the power flowing into the divertor, leading to higher radiative losses. In addition, the dependence of the carbon erosion on particle flux and impact energy may contribute to keeping the divertor radiation resilient to strong variations of the input power.

The modified divertor geometry also strongly influences the compression (defined as $n_{0,div}/n_{ion,edge}$) of deuterium as well as helium, as was predicted by B2-EIRENE modelling [8]. For both ion species, the compression ratio in Div II is much larger than in Div I, resulting in practically identical enrichment ratios for helium [9] and identical values for $\rho^* = \tau^*_{He}/\tau_E = 4\ldots6$.

3. Confinement physics

3.1. Confinement identity in ASDEX Upgrade and JET

Confinement identity experiments were conducted in ASDEX Upgrade and JET [10] in which the dimensionless variables $(\rho*, \nu*, \beta)$ and plasma shape were made the same. As expected, $B_t\tau_E$ is the same in the two devices at low density but not at high density ($\bar{n}_e/n_{GW} \approx 0.8$). It seems therefore that the physics of confinement degradation with increasing density, which is related to edge effects (Sect. 5 and Ref. [11]), is not necessarily compatible with the invariance principle, at least not in the form used here. This is supported by the analysis of profiles which at both low and high density exhibit a good match of density and temperature and therefore of $\rho*, \nu*$ and β. However, it reveals that the NBI power deposition

profiles were significantly more peaked in JET than in ASDEX Upgrade, leading to a factor of about 2 difference of the heat fluxes at mid-radius. This leads to a corresponding difference of diffusivity although the dimensionless parameters are quite similar.

3.2. Transport studies with ECRH

On- and off-axis ECRH has been applied to ohmically heated plasmas. Between 300 kW and 600 kW of RF power was injected at about mid-radius into discharges with about 800 kW of ohmic heating. On top of this, a 10% power modulation at 30 Hz was added to study the behaviour of transient transport. Comparing on- and off-axis injection, the temperature profiles remain quite peaked in the off-axis case. Analysis of the power balance and heat pulses launched by modulated ECRH indicate a strong transport reduction in the central region, between the ECRH deposition and the plasma axis, to sustain such peaked profiles. The possibility of an anomalous inward heat pinch can be ruled out.

Heat pulse propagation from ECRH modulation and sawteeth was compared over a large range of plasma parameters [11] with NBI background heating up to 5 MW and hydrogen or deuterium gas. The ratio of the heat pulse (χ^{HP}) and power balance (χ^{PB}) diffusivities in deuterium strongly increases with heating power up to about 10 (ECRH modulation), while it is 15 for sawtooth heat pulses at $P_{heat} = 5$ MW. This suggests that transport might be determined by a critical gradient effect. The ratio χ^{HP}/χ^{PB} in hydrogen exhibits a weaker increase with heating power up to a value of 3. Generally, it is observed that χ^{HP} from sawteeth is up to twice as high as that from ECRH modulation.

3.3. Profile saturation and isotope effect

For both isotopes a temperature profile saturation with increasing heating power is observed in ASDEX Upgrade. The stationary high-power deuterium data well below $\overline{n}_{GW}$ fit the thermal ITER ELMy H-mode scalings. The hydrogen data show an even stronger confinement decay with increasing power which is only compatible with the scaling if a (log-linear) interaction term for the power and isotope mass A_i is included [12]. For a pair of discharges with identical global parameters except for A_i and the same density profiles the variation of the confinement was a factor of two larger than expected from the scaling. The corresponding T_e profiles differ by a radially constant factor, exhibiting "stiffness" as described in Sect. 5.

4. H-mode threshold

The scaling and physics of the H-mode threshold has been investigated in ASDEX Upgrade in various regimes [13,14]. With Div II, the H-mode power threshold, expressed in terms of $\overline{n}_e \times B_t$, has increased by about 20 %. However, the dependence on the edge density is unchanged and the scaling difference originates from a slightly different density profile peaking in the two geometries, which is generally visible in L-mode. The critical edge temperature for the H-mode transition in hydrogen and deuterium plasmas differs by only about 20 % for similar parameters, i.e much less than the heating power isotope effect of a factor of 2. A simple scaling has been found which describes the H-mode threshold in local edge parameters [15,16] even in cases where the power threshold diverges.

Identity experiments in JET and ASDEX Upgrade have been used to test the compatibility of local parameters at the L-to H transition with Kadomtsev constraints [10,17]. B_t, I_p and the edge density are adjusted to match dimensionless parameters in the two machines of different size. Unlike in confinement similarity studies, the heating power cannot be varied in order to achieve a match, but is defined by the occurrence of the H-mode transition. Thus, in principle, only 2 out of 3 dimensionless parameters ρ^*, β and ν^* can be matched. It was found, however, that ρ^* and β at the transition depend only weakly on ν^* and all three parameters can be simultaneously matched . Figure 4 shows that even the T profile shapes at the L-H transition satisfy the core Kadomtsev constraints. This demonstrates compatibility with the Kadomtsev constraints, e.g. all H-mode physics models based entirely on Fokker-Planck and Maxwells

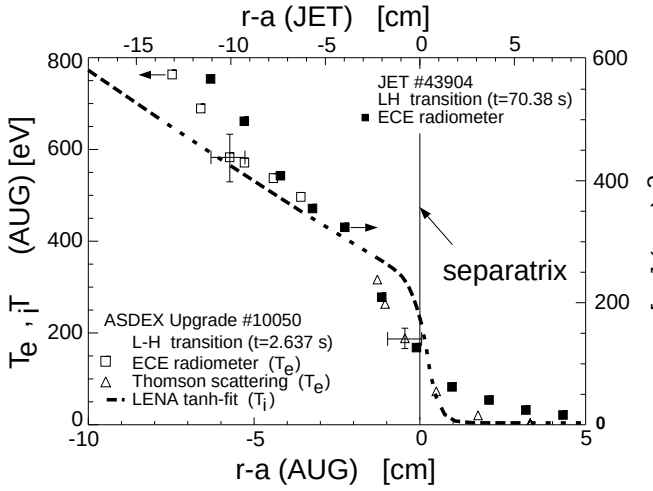

Figure 4: Edge temperature profiles in ASDEX Upgrade (left scale) and JET (right scale) at the L-H transition. These edge profile shapes satisfy the Kadomtsev constraint and scale as $T_{edge} \sim R^{-0.4}$.

equations. An alternative assumption of atomic physics being relevant, e.g. via ionization or charge exchange processes, would lead to a different scaling of dimensional parameters with size [18].

H-mode theories which aim at explaing the driving and inhibiting forces for the observed build-up of the radial electric field E_r [19] have been tested on ASDEX Upgrade. A quantitative comparison of the neutral friction force, using 2D EIRENE Monte Carlo neutral transport calculations, with neoclassical viscosity has been done in full geometry [20]. In typical medium-density cases, the neutral forces are weak and can affect E_r only through their effect on toroidal rotation. Due to experimental uncertainties, in particular in the mutual alignment of various measured edge profiles, it is very difficult to estimate orbit effects. Monte Carlo charged-particle calculations in full ASDEX Upgrade flux surface geometry show that the ion orbit loss current may account for the driving forces needed to compensate for the effect of neoclassical viscosity [21] at $\nu^* \approx 1$. However, experimentally the H-mode transition is achieved in a wide range of collisionalities, ranging up to much higher values. A possible driving mechanism of $E \times B$ rotation is Reynold stress due to the turbulence which causes anomalous transport. Various simulations of edge transport in the drift-Alfvén-ballooning regime relevant at the plasma edge have been performed [22–24], but so far no definite picture exists on whether such an effect is obtained in a local model or not.

In ASDEX Upgrade, for powers ranging from 2.5 to 5 MW, with the plasma far into the H-mode (1.5 to 3 times the threshold power, clear type I ELMs), no differences were observed in the ELM behaviour between NI and ICRF heated plasmas. Not only is the ELM frequency at the same power and density identical, but the average edge electron temperature (near the separatrix, $0.95 \leq \rho_{pol} \leq 1.05$) and the amplitude of the variation of the edge electron temperature due to the ELMs are the same [2,25].

5. High density H-mode operation

Dedicated experiments over a wide range of plasma parameters are carried out in ASDEX Upgrade to investigate confinement and operational limits. The H-mode density limit [26] is closely connected with a back-transition to L-mode, followed by the typical L-mode density limit scenario [27], full detachment, MARFE expansion onto the closed flux surface, resistive MHD and eventually disruption. This sequence is routinely interrupted in ASDEX Upgrade, where after detection of an expanding MARFE the control system automatically increases the heating power and cuts off the gas puff, thereby avoiding a density limit disruption. As a final protection method, an impurity-doped "killer pellet" or high gas puff is used to mitigate the disruption.

A wide parameter range ($I_p = 0.4 \ldots 1.4$ MA, $B_t = 1.3 \ldots 3$ T, $P_{NBI} = 2.5 \ldots 20$ MW) was used together with controlled optimum heating-power-dependent neutral-gas flux to identify scalings with increased precision. At high densities, core fuelling by gas puff becomes inefficient, and the density profile flattens with increasing fuelling rate (see below). Figure 5 (a) shows the measured heating power dependence of the density limit, normalized as a first approximation to the Greenwald density n_{GW} [29]. The power is normalized to $P_{thr}(\overline{n}_e = n_{GW}) \propto n_{GW} B_t \propto I_p^2 q$ to reflect the L-H transition power threshold found at

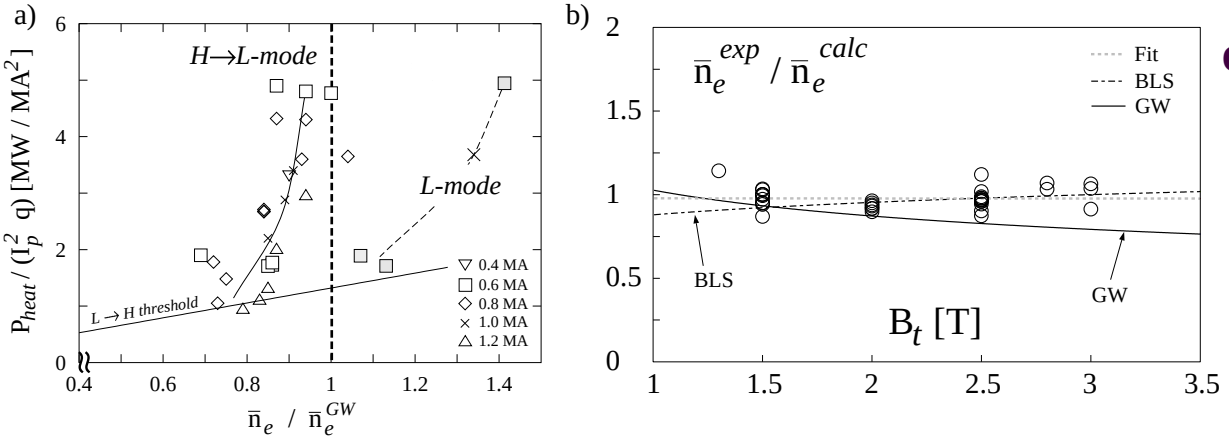

Figure 5: (a) H-mode and L-mode density limits in global operation space, showing a strong deviation of the H-L back-transition from the $P_{thr} \propto \bar{n}_e B_t$ scaling near $\bar{n}_e^{GW}$, (b) comparison with boundary layer (BLS, Ref. [28]) and Greenwald scalings in a B_t scan (see text).

low and medium densities ($P_{thr} \propto \bar{n}_e B_t$) extrapolated to the Greenwald density $n_{GW} = I_p/\pi a^2$. At high density, the heating power needed to stay in the H-mode increases significantly above the threshold scaling at lower densities, resulting in a weak power dependence of the H-mode density limit, $n_e^{exp} \propto P_h^{0.15}$ [5]. The wide parameter variation can be used to test more-physics-based scalings derived from edge physics, e.g. the H-mode density limit scaling proposed in Ref. [28] on the basis of boundary layer transport at the onset of detachment (BLS, $n_e^{BLS} \propto P^{0.1} B_t^{0.53}/q_{95}^{0.9}$) in comparison with the Greenwald scaling (GW, $n_e^{GW} \propto B_t/q_{95}$). As the two scalings differ mostly in their B_t dependence, a B_t scan is used for discrimination. Figure 5 (b) shows fits to the experimental data n_e^{exp}, individually normalized to the scalings (curves) and the residuals with respect to a fit to the data points alone (circles). This fit yields $n_e^{exp} \propto P^{0.15} B_t^{0.6}/q_{95}^{0.95}$, which is close to the BLS model and has a noticeable difference to a pure Greenwald-type scaling. Local edge parameter measurements [30] reveal that near the H-mode density limit the onset of detachment in between and during type-III ELMs occurs at edge collisionalities close to those encountered at the H-L back-transition. The back-transition itself is recognized as a breakdown of the temperature gradient (edge transport barrier) inside the separatrix. It is not clear whether this apparent change of radial transport has a causal relation to the detachment or is caused by an independent mechanism. One possibility might be a collisionality dependence of anomalous transport at high edge β (near the ballooning limit). Current transport simulations disagree whether this effect is created locally by drift-Alfvén-ballooning turbulence [22] or not [23].

For densities raised towards the density limit, confinement deterioration with respect to H-mode scaling laws and reduction of stored energy are found [16]. This is illustrated in Fig. 6 a for a density ramp experiment, where the neutral-gas flux and the heating power were raised together to avoid MARFE formation. Even with increased heating power, the H-factors relative to L-mode ($H_{ITER89P}$) and ELMy H-mode ($H_{ITER92Py}$) decrease by about 50% when a density of 90% n_{GW} ia approached. The origin of this degradation can be inferred from the profiles, taken at 3 different times, demonstrating that this deterioration is due to an edge-core relation via stiff temperature profiles. Increasing the density by gas puff, the main density rise takes place at the edge, leading to flattening of density profiles (Fig. 6 b). In regimes with sufficient heating power flux, e.g. in type I-ELMy H-mode or in type III-ELMy phases with high power near the H-mode density limit, a limitation of the logarithmic gradient $T'/T = 1/L_T$ is observed [11,15], independent of (varying) power deposition profiles, radiation profiles, gas puff and density range. The self-similar profiles lead to a relation $T(0) \propto T_{edge}$. With increasing edge density, the pressure gradient limit due to ELMs, in conjunction with a fixed edge pedestal width, forces a reduction of edge temperature, which in turn leads to reduction of the core temperature (Fig. 6 c). Shown are ion temperatures, but the same observation is made for electron temperatures as well. As the density profile is essentially flat, a reduction of the volume-integrated pressure or thermal stored energy results.

One can expect to achieve improved confinement if high core and low edge densities can be combined, i.e. if a significant density gradient can be maintained in the confined plasma. This is achieved by pellet injection, in particular from the high-field side [5,31], which results in improved fuelling effi-

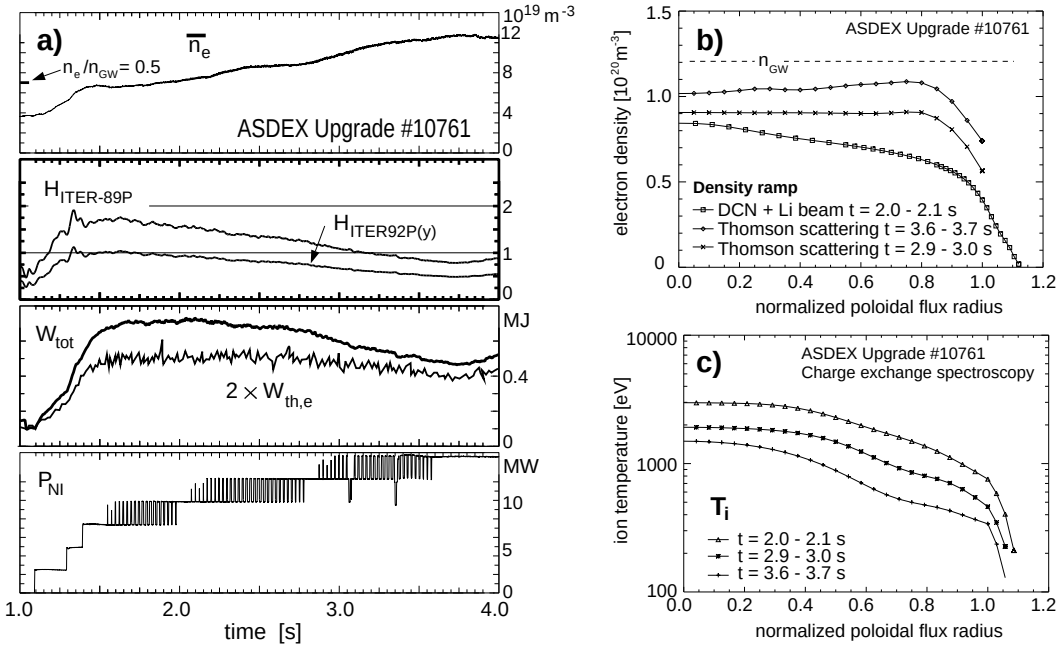

Figure 6: Time traces (a), Density (b) and ion temperature (c) profiles for a density ramp experiment. With increasing edge density, the edge temperature and core temperature drop, leading to deterioration of confinement.

ciency and deeper pellet penetration compared with injection from the low-field side with the same pellet parameters. Figure 7 (a) shows density profiles in the course of a pellet train. The edge density gradient zone is extended into the core plasma, leading to a larger core density with a moderate increase of the edge density. Compared with gas puff, first a much higher density well above the Greenwald density limit can be achieved. Secondly, at any given density, improved confinement is found (Fig. 7 b), but the envelope of all pellet discharge trajectories still indicates a reduction of confinement with increasing density, in contrast to the prediction of the ITER H92P(y) confinement scaling. While at low heating powers, high confinement can be achieved together with operation well above n_{GW}, at high heating power the energy content decreases with increasing density already below n_{GW}. This is at least partly due to the fact that core temperature profiles are limited by the edge pressure gradient, which has a very weak power dependence [32].

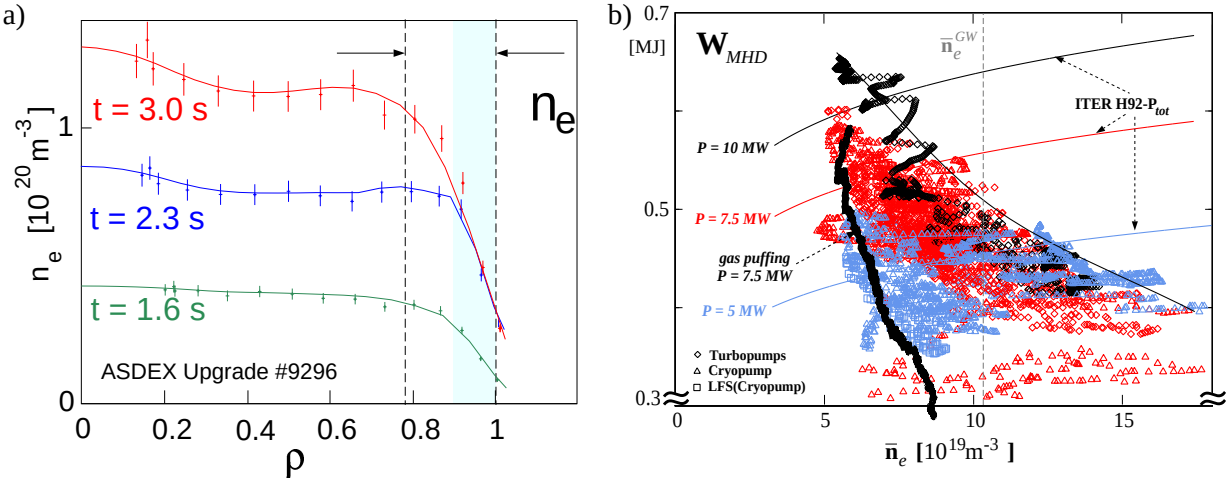

Figure 7: Pellet injection from the high-field side: (a) Density build-up during a train of pellets, (b) MHD stored energy vs. density from trajectories of discharges with different heating powers.

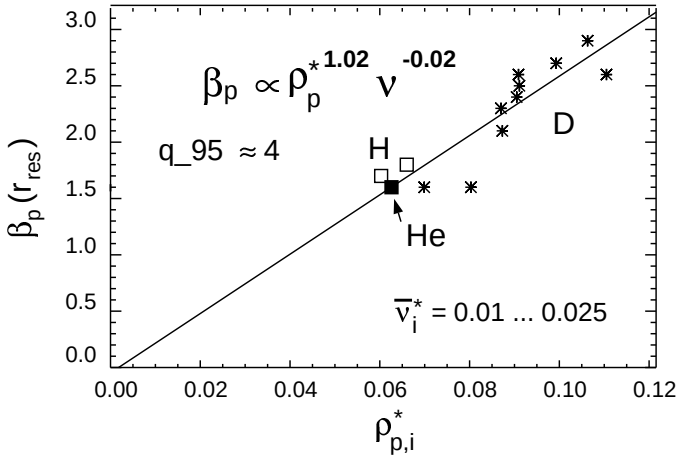

Figure 8: β_p at the rational surface q = 3/2 at the time of the mode onset versus ρ_p^* for collisionless plasmas of H, D, and He ($\nu_{eff} < 1$; $q_a = 4....4.4$).

6. Neoclassical tearing mode studies and ECCD feedback stabilization

The onset of neoclassical tearing modes (NTMs) leads to the most serious β limit in ASDEX Upgrade. The β_p value for the onset of such modes is found to be proportional to the ion gyro-radius for collisionless plasmas as proposed by the ion polarization current model [3]. Within this model one arrives at $\beta_{p,onset} \propto g(\varepsilon,\nu_{eff})\cdot\rho_p^*$ with $g(\varepsilon,\nu_{eff}) = \varepsilon^{3/2}$ for $\nu_{eff} \ll 1$ and 1 for $\nu_{eff} \gg 1$ ($\nu_{eff} = \nu_{ii}/(m\varepsilon\omega_e^*) \sim \nu^*/\rho^*$). ω_e^* is the electron diamagnetic drift frequency. In Fig. 8,the onset conditions in the much more unstable collisionless regime $\nu_{eff} \ll 1$ are represented, and the $\beta_{p,onset} \propto \rho_p^*$ scaling on ion mass is shown for different species. Using the stabilizing effect of higher collisionalities, a scenario was developed for plasma discharges at high density with large heating power and energy content in which the limiting (3/2)-mode can be avoided in ASDEX Upgrade. As shown in Fig. 9, this scenario has allowed stationary high values of β [33].

Only islands larger than a minimum "seed" island have positive growth rates. In ASDEX Upgrade the seed island is often produced by sawteeth, although sometimes neoclassical modes start after fishbones or even grow spontaneously [34]. Although the seed island creation by the (2,2)-precursor of a sawtooth is regarded as the most common mechanism for the triggering of NTMs, in ASDEX Upgrade it has been found that the sawtooth crash produces a (3,2)-seed island directly, without a coupled (2,2)-mode. Since fishbones are usually regarded as an ideal instability, acting only on the fast particle distribution, they should not be able to produce magnetic reconnection [35]. Nevertheless, it has been shown that fishbones do change the temperature of the background plasma on a much faster time scale than would just follow from the redistribution of the fast particles and the accompanying reduced heating power. For an NTM following fishbones, β_p is higher than in cases with a sawtooth trigger, indicating that fishbones are less efficient than sawtooth crashes in producing seed islands [34].

The degree of confinement deterioration due to neoclassical tearing modes has been investigated and compared with corresponding numerical simulations [36]. The fractional energy loss due to a (3,2)-mode was found to saturate for high pressures at around 25 %, which is in good agreement with the theoretical results. Thereby the theoretically derived saturation of the island width with plasma pressure, the confinement deterioration with increasing island width and the observed density decrease influencing the energy confinement as described by the ITER-97P H-mode scaling have been combined.

Since neoclassical islands are driven by the vanishing bootstrap current inside the island, the growth of these modes can be influenced by phased heating and current drive into the O-point of the island. Recently, a reduction in amplitude of a neoclassical (3,2) tearing mode and partial recovery from an initial drop of β by 40 % were been achieved in ASDEX Upgrade by using modulated ECCD/ECRH [4,38] with a maximum pulse length of 200 ms, see Fig. 10. The resonance position was adjusted according to the island location detected by ECE. The ECCD timing was controlled by Mirnov signals of the modeing such a way as to drive current only in the island O-point.

In numerical simulations, including an externally driven current into Ohm's law, one finds that stabilization of neoclassical tearing modes should be possible if the external current replaces the missing bootstrap current inside the island [37]. The driven current has been calculated using a dynamic model

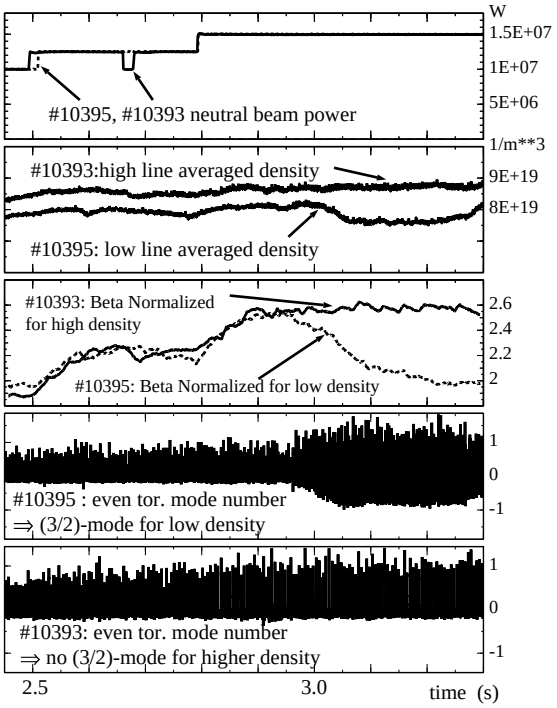

Figure 9: Dependence of the excitation of the neoclassical (3,2)-mode on the collisionality alone. β_N remains constant while the density decreases and $\nu_{ii}/m\varepsilon\omega_e^*$ is slowly reduced until its threshold is reached.

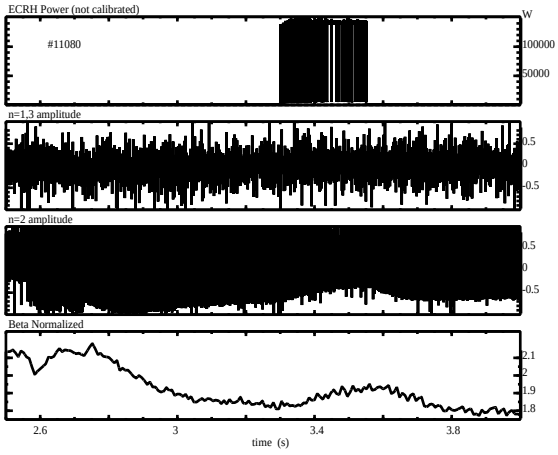

Figure 10: Active control of the neoclassical tearing mode with O-point ECCD. The smooth reduction of the mode amplitude is accompanied by an increase in β_N.

based on a 3D Fokker-Planck code coupled to the electric field diffusion and the island evolution equations. The stabilization efficiency strongly depends on the width of the driven current layer. If the current layer width is small enough, one can completely stabilize the island since the pressure is not completely flattened across small islands, resulting in a reduced driving term due to the smaller helical hole in the bootstrap current.

7. Advanced tokamak operation

Improved core confinement due to modification of the current profile has been observed in several tokamaks. Common to these regimes of operation is the flattening of the central current profile corresponding to a zero or even negative value of the central magnetic shear (s = $\frac{r}{q}\frac{dq}{dr}$, where q is the safety factor). There is increasing evidence that, in addition to magnetic shear stabilization, a combination with $E \times B$ shear stabilization is required for the initiation of internal transport barriers (ITB) [39,40].

On ASDEX Upgrade, various operating scenarios have been tested to achieve improved core confinement by modifying the current density profile by means of early additional heating in the current ramp to reduce current diffusion at low initial density ($\bar{n}_e < 3 \times 10^{19}\ m^{-3}$):

1) ITBs with an H-mode edge in combination with a flat, but still hollow, q-profile with $q_0 \geq 1$ are obtained, which offer stationary, inductively driven H-mode operation with increased performance in terms of confinement and β. Such q-profiles with $q_0 \approx 1-1.5$, resulting in l_i values above 0.8 at $q_{95} \geq 3$ together with broad pressure profiles ($p_o/ < p >< 3$), help to avoid ideal kink modes occurring at $\beta_N \geq 4l_i$ without wall stabilization. β_N values between 3 and 4 would be possible, if the neoclassical tearing modes unstable under these conditions for $\beta_N > 2.2$ could be stabilized by active feedback control as described in the previous section. Plasma shapes with higher elongation κ and triangularity δ than those now being used in ASDEX Upgrade ($\kappa < 1.8, \delta < 0.2$) should help by reducing Δ'.

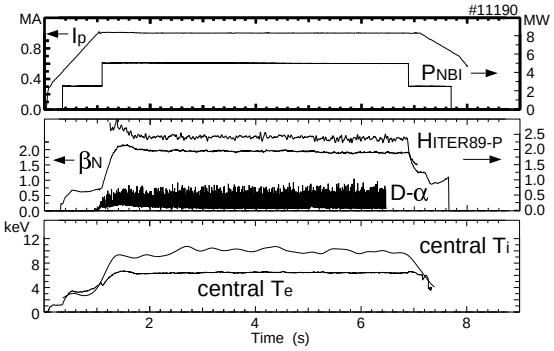

Figure 11: Time evolution of plasma current (I_p), neutral beam heating power (P_{NBI}), H-factor ($H_{ITER89-P}$), normalized beta (β_N), divertor D radiation, and central electron and ion temperatures ($T_{e,i}$) for a stationary discharge with ITB and H-mode edge. The toroidal magnetic field is B_{tor} = 2.5 *T*.

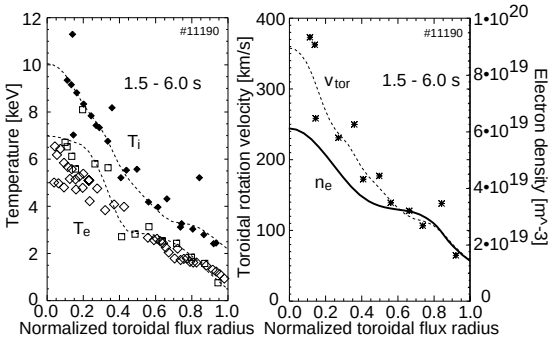

Figure 12: Radial profiles of ion and electron temperatures, electron density, toroidal rotation velocity (v_{tor}) of the discharge presented in Fig. 11. The profiles are the average from 1.5 to 6 *s* covering most of the 5 *MW* heating phase.

2) ITBs with reversed shear and q_{min} values above 2 could only be transiently established in ASDEX Upgrade both with plasma edge parameters comparable to L-mode and with an H-mode edge. Here, ITBs with L-mode edge are distinguished by steep pressure gradients in the barrier region, while discharges with improved core confinement and H-mode edge exhibit more moderate gradients. These current profiles would offer the route for true steady-state, non-inductively driven tokamak operation combining improved performance and high bootstrap current fraction $f_{bs} = I_{bs}/I_p \propto \beta_N q_{95}\sqrt{A}$, at high $q_{95} \geq 4$ and $\beta_N \geq 4$. Low (m,n) neoclassical tearing modes are avoided by the reversed shear and $q_{min} > 2$, but ideal kink modes are already unstable at low β_N values due to the broad j-profile with low l_i values. Wall stabilization, broad pressure profiles and plasma shapes with high elongation and triangularity are therefore needed to achieve $\beta_N \geq 4$. The possibly arising resistive wall modes would again need active feedback control by coils creating toroidal n=1 and 2 components at the wall.

7.1. Stationary H-mode with improved core confinement

A stationary regime of operation has been found which shows improved core confinement of both electrons and ions caused by an internal transport barrier (ITB) in combination with an H-mode edge [41]. In Fig. 11, the main plasma parameters of such a discharge are illustrated. During the current ramp of 0.8 MA/s moderate neutral beam heating of 2.5 MW is applied. At $t = 1$ s the X-point is formed and the L-H-transition occurs. After the current flat top is reached, the NBI power is raised to 5 MW and the line-averaged density is kept at 4×10^{19} m^{-3}.

While the electron and ion temperatures increase at the same rate during the current ramp at a heating power of 2.5 MW, T_i reaches almost twice the value of T_e when the heating power is doubled. Central values of $T_i = 10$ keV and $T_e = 6.5$ keV, $H_{ITER89-P} = 2.4$, and $\beta_N = 2$ are maintained for 6 s, only limited by the programmed duration of the NBI. This corresponds to 40 confinement times or 2.5 resistive time scales for internal current redistribution, which here is the time taken by a current perturbation to diffuse over half of the minor radius. The perturbation was assumed to be located inside the half-radius region and to conserve the total plasma flux. The 8-channel motional Stark effect (MSE) polarimeter data show that the current profile remains stationary shortly after the full neutral-beam power is applied. In addition, the measured loop voltage is also stationary within 10 %. These discharges resulted in the highest value of $n_{D,0} \times T_{i,0} \times \tau_E$ (7.5×10^{19} keV s m^{-3} for 6 s and 8×10^{19} keV s m^{-3} for 1 s) so far observed on ASDEX Upgrade.

The profiles of the plasma temperature, density and toroidal rotation velocity (see Fig. 12) show, in addition to the H-mode pedestal, a step starting at ρ_{tor} = 0.6 which, compared with ASDEX Upgrade

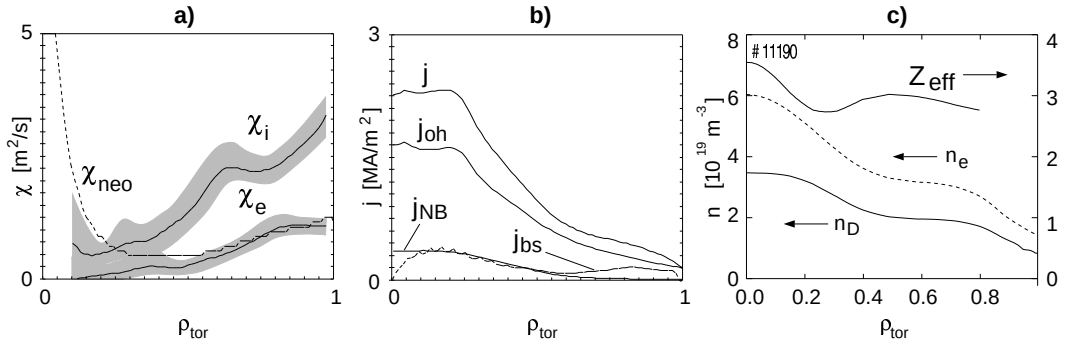

Figure 13: Radial profiles from ASTRA analysis for stationary ITB discharge with H-mode edge (at 2.5 s of # 11190). a) Ion and electron thermal conductivity. b) Composition of current profile. Shown are the total current density and the contributions of ohmic current (oh), neutral-beam current drive (NB) and bootstrap current (bs). c) Radial profiles of electron and deuteron densities, and Z_{eff} at 4 s of discharge # 11190. The Z_{eff} profile represents an upper limit.

transport barriers with L-mode edge, is less pronounced. The density peaking is $n_{e,0}/\overline{n}_e$ = 1.5. Energy transport has been analyzed with the 1-1/2-D ASTRA code. In the central regions of the plasma the ion thermal conductivity drops to neoclassical values, but also the electron thermal conductivity is at a low level, indicating that the transport reduction is not limited to the ions, as seen in Fig. 13.

The only MHD activity observed in the core of the plasma is strong (1,1) fishbones which start at 1.1 s at $\rho \approx 0.2$ and accompany the entire 5 MW heating phase, indicating that the central q is in the vicinity of one; but not low enough for the formation of sawteeth. These fishbone oscillations seem to behave like a resistive MHD instability [35]. Similar to sawteeth, but on a much faster time scale of 1 ms, the soft X-ray (SXR) and T_e (from ECE) profiles show a relaxation oscillation expelling energy and possibly also impurities. The magnetic reconnection due to fishbones would also explain that, despite q being in the vicinity of one, sawteeth do not appear, since the fishbone oscillations could serve as a mechanism for keeping q at one. This is supported by the ASTRA calculations, which solve the current diffusion equation using the experimental temperature and Z_{eff} evolution, using Kadomtsev reconnection, which redistributes the central current as soon as q drops below one. The resulting q-profile is flat in the centre with $q \approx 1$ inside $\rho_{tor} = 0.2$, which is consistent with the location of the (1,1) fishbone mode derived from the SXR oscillations. Without this mechanism a stationary current profile is not attained in the transport calculation.

The composition of the current density profile from ASTRA is illustrated in Fig. 13 b. The total current profile is flat in the centre, but still monotonic, which is supported by the bootstrap current having its maximum close to the centre due to a smaller pressure gradient as compared with internal transport barriers with L-mode edge. These stationary discharges with ITB are mainly inductively driven ($U_{loop} = 0.15$ V) and exhibit on-axis peaked ohmic, bootstrap and beam ion driven currents. The moderate bootstrap current fraction of 25% of I_p is due to the $\beta_N = 2.2$ limit for this scenario, which, however, offers a potential for long-pulse, stationary operation with high central $n\tau T$ values and good performance.

The impurity content and Z_{eff} profiles are slightly peaked in the plasma centre (see Fig. 13 c) , but no temporal accumulation is observed from 2 s until the end of the 5 MW heating phase. From spectroscopic data the main impurities have been identified as helium (He: 5%), carbon (C: 2.5%), oxygen (O: 1.2%) and silicon (Si: $\approx$ 0.3%) after siliconization of the vacuum vessel. Neglecting the presence of elements with Z larger than Si, an upper limit of Z_{eff} was inferred from SXR emission by using an impurity transport code. The peaking of the electron density is partially caused by the impurities, but nevertheless the deuteron density also increases towards the plasma centre. The steady-state is possibly caused by the strong fishbone activity expelling, like sawteeth, impurities from the plasma core.

If the density is increased at constant heating power, sawteeth appear and the ITB is lost but is restored as soon as the gas puff and density are reduced. This may be due to 1) a density dependence of the ITB power threshold, 2) an effect of T_i/T_e variation, where T_i approaches the nearly unchanged T_e, or 3) the

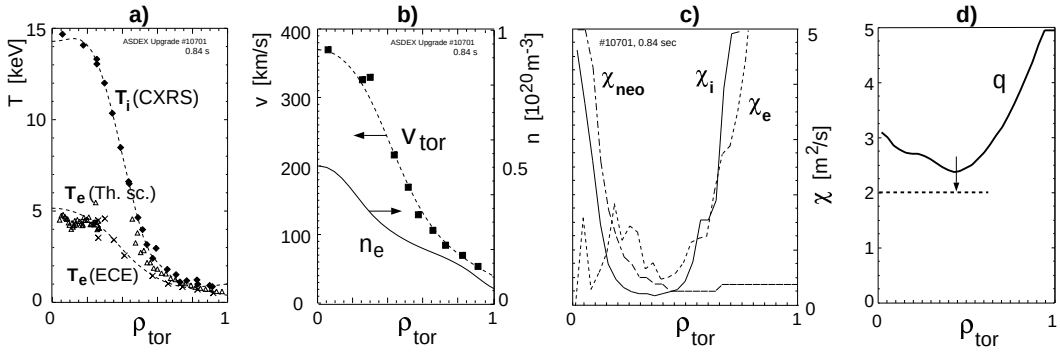

Figure 14: Radial profiles of ion and electron temperatures (ECE and Thomson scattering), electron density, toroidal rotational velocity (v_{tor}) of discharge with ITB, L-mode edge, and reversed shear with $q_{min} > 2$. The time point chosen is at maximum performance just before termination of the ITB. The ion and electron thermal conductivities ($\chi_{i,e}$) from ASTRA analysis are compared with the neoclassical ion thermal conductivity (χ_{neo})[10]. The calculated q-profile is given in d).

increase of neutral particle flux and simultaneous decrease of density peaking.

When increasing the beam power, β_N is limited by the occurrence of (3,2) neoclassical tearing modes, the onset of which is always preceded by a fishbone. Considering that sawteeth are not present, the second harmonic of a (1,1) fishbone acts as a seed island for the initiation of (3,2) neoclassical tearing modes [3]. The resulting β-limit is close to β_N = 2.2. At 6.25 MW of NBI, β_N = 2.2 could still be maintained for a duration of 1 *s*, after which a (3,2) mode occurred due to the proximity to the β-limit. With further increased heating power (up to 10 MW), transient phases with higher $\beta_N \rightarrow 3$ and $H_{89P} \rightarrow 3$ are observed which are terminated by neoclassical tearing modes. Due to the low density, the (3,2) modes were usually followed by (2,1) modes which ultimately lock.

7.2. Internal transport barrier with reversed shear and $q_{min} > 2$

Applying 5 MW of NB heating power during the I_p ramp of 0.8 MA/s has yielded transient reversed-shear plasmas with ITB's during this ramp-up phase. These ITB phases were usually terminated by (2,1) modes already, when the plasmas still possessed an L-mode edge due to the initial limiter phase. The H-mode transition occurring with the ion (∇B) drift towards the forming X-point only reduced the connected β-drop.

Avoiding the H-mode transition by staying in limiter configuration has yielded, high reversed-shear plasmas with ITB's and central values of $T_e = 5$ keV and $T_i = 15$ keV. The confinement enhancement factor of $H_{ITER89-P} = 1.9$ and normalized beta of $\beta_N = 1.6$ are limited by both the smaller radial extent of the barrier region ($\rho_{tor} < 0.5$) and the L-mode edge.

Figure 14 shows the profiles of the temperature, density, toroidal rotational velocity, and q of such a discharge with L-mode edge and ITB. Associated with the high ion temperatures are toroidal velocities of up to 370 km/s. Transport analysis again shows that the ion thermal conductivities are at neoclassical values in the plasma core. The plateau in T_i leads to the rise of χ_i towards the plasma centre, the uncertainty of which is large (50%) since it sensitively depends on the T_i gradient there. Such ion thermal transport enhancement near the magnetic axis might be explained by including finite orbit corrections to χ_{neo} since the measured E_r field leads to an ion orbit increase counteracting the orbit squeezing effect in this region. The electron thermal conductivity inside the barrier is larger than χ_i, as reflected in the large difference between T_i and T_e, which is only partially caused by the stronger NBI heating of the ions.

The q-profile, inferred from the transport calculations, exhibits a negative central shear region with $q_{min} > 2$. The limiting (2,1) mode, presumably an external kink mode, occurs as soon as a $q = 2$ surface is formed due to the constantly penetrating current. This is supported by the increasing time delay for the mode occurrence of about 0.4 s when the toroidal field was enhanced from 2 to 2.8 T at $I_p = 1$ MA.

The following conclusions can be drawn from the comparison between the more closed Div II and the more open Div I configurations. No major changes occurred in the typical high-power density ramp-up scenarios, this including similar values for the upper density limit in H-mode and the ultimate L-mode density limit. However, as expected the divertor neutral density is higher in the more closed Div II, leading to detachment at lower densities. A strong improvement of the helium exhaust efficiency has been achieved, affording a ratio $\tau^*(\mathrm{He})/\tau_E \approx 4\ldots6$.

The most important observation in the Div II geometry is a strongly distributed power flux to the surrounding structures both during ELM and ELM-free phases. Even with a heating power of 20 MW the maximum local heat flux density in the strike point region stays below 5 MW/m^2. The origin of this reduction by a factor of about three compared with Div I is a larger fraction of divertor radiation (up to 55 % of the heating power) due to increased cooling by hydrogen and carbon radiation in this divertor geometry. This result is in agreement with B2-Eirene simulations and may have a strong influence on the future divertor designs.

Several new results have been obtained in the confinement and performance related physics. The characterization of the L-H transition in terms of local edge parameters clearly indicates a minor influence of the collisionality. A result from the ASDEX Upgrade-JET dimensionless identity experiments is that the L-H transition is compatible with core physics contraints ($\rho*, \nu*, \beta$) and shows no evidence of direct influence from atomic physics processes. ELM frequencies were found to be rather independent of the heating method up to 6 MW (a factor of 2.5 above the L-H transition power) when using either NBI or ICRH minority heating.

One of the main focuses of our work was an ITER-relevant ELMy H-mode scenario close to the operation limits, namely density and β-limits, where the confinement is strongly influenced. While the H-mode transition can be reached up to high collisionalities and densities close to the Greenwald density, although with finally drastically enhanced threshold power, the H-mode confinement degrades strongly in relation to ITER-92P scaling. The reported temperature profile resilience might be caused by turbulent convection relating the plasma parameters at the edge transport barrier to the core parameters. As a consequence, the achievable core temperatures and pressures degrade at high densities because the achievable edge pressure and its gradients are limited by the edge ballooning mode. Stationary H-mode operation at densities 20 to 40 % above the Greenwald density was demonstrated with pellet refuelling from the high-field side. The higher densities compared with gas puff-refuelled plasmas are due to widening of the density gradient region inside the separatrix. These pellet-refuelled plasmas have better confinement than gas-puff-fuelled ones, in general. At low heating powers, high confinement is maintained up to the highest densities, but at high heating power a reduction of confinement with increasing density is again found.

At high heating powers, neoclassical tearing modes, mainly (3/2) modes but also (2/1) modes at lower densities, limit the achievable β, but also fishbones may be a limiting factor, depending on the collisionality at the resonant q-surfaces. At high densities and therefore high collisionality neoclassical modes can be suppressed, allowing slightly higher β_N. The seed island size necessary for the growth of neoclassical modes decreases at higher β values, while at lower β a big seed island triggered by a sawtooth is necessary. Spontaneous, but slowly growing neoclassical modes have also been observed. The measured saturated island width and the scaling with ρ^* and ν^* agree with theoretical MHD calculations for the polarization model. For the first time, neoclassical tearing modes have been actively stabilized by feedback-controlled ECCD into the island's O-point. This feedback stabilization scheme has a high potential for next-step devices since the ECRH powers required are only a few per cent of the applied heating power and the driven currents in the islands are only 1 % of the total plasma current. New MHD phenomena were observed, resistive interchange modes with centrally inverted pressure profiles and cascades of high-n tearing modes in flat shear regions [42].

In advanced tokamak scenarios strongly reduced core transport was achieved with flat shear profiles and $q(0) \geq 1$ or with reversed shear and $q_{min} > 2$, created by freezing the current profile with 'early' heating (ECRH, ICRH, NBI) during current ramp-up, which was followed by stronger central heating with up to 10 MW NBI in the flat-top. A stationary H-mode scenario with internal transport barriers for ions, electrons, particles and toroidal momentum, $H_{ITER-89P} = 2.4$ and $\beta_N = 2.0$ was maintained for 40 con-

finement times and several internal skin times. Highest $n_i T_i \tau_E$ values of 8×10^{19} keV s m-3 (for 1 s) observed so far in ASDEX Upgrade were obtained in these discharges. Both ion and electron transport were strongly reduced inside the barrier region, and no temporal accumulation of impurities was observed. The stationarity of the discharges is associated with a fishbone induced stabilization of the current profile occuring with small scale perturbations, which in contrast to sawteeth are compatible with improved confinement. Attempts to increase β_N were limited by either (3,2) neoclassical tearing modes in the case of flat q profile or (2,1) modes with reversed shear profile by approaching $q_{min} = 2$.

During the next years, investigations will be continued with enhanced capabilities for plasma shapes with higher triangularity ($\delta \rightarrow 0.45$), off-axis current drive ($\leq$ 400 kA, by NB-CD with 100 keV D^0 and ICCD using mode conversion) and extended pulse lengths of up to 10 seconds.

References

[1] BOSCH, H.-S. et al., Extension of the ASDEX Upgrade programme: Divertor II and tungsten target plate experiment, Technical Report 1/281a, IPP, Garching, Germany, 1994.

[2] NOTERDAEME, J.-M. et al., in *Europhysics Conference Abstracts (Proc. of the 2nd Europhysics Topical Conference on Radio Frequency Heating and Current Drive of Fusion Devices, Brussels, 1998)*, volume 22A, pages 9–12, EPS, 1998.

[3] GÜNTER, S. et al., Nucl. Fusion **38** (1998) 325.

[4] ZOHM, H. et al., post dead-line paper, this conference.

[5] MERTENS, V. et al., paper IAEA-CN-69/EX3/6, this conference.

[6] KAUFMANN, M. et al., paper IAEA-CN-69/EX3/2, this conference.

[7] HERRMANN, A. et al., in *Europhysics Conference Abstracts (Proc. of the 23rd EPS Conference on Controlled Fusion and Plasma Physics, Kiev, 1996)*, volume 20C, part II, pages 807–810, Geneva, 1996, EPS.

[8] SCHNEIDER, R. et al., paper IAEA-CN-69/THP2/05, this conference.

[9] BOSCH, H.-S. et al., Effect of divertor geometry on boundary and core plasma performance in ASDEX Upgrade and JET, to be published in Plasma Phys. and Contr. Fusion.

[10] RYTER, F. et al., paper IAEA-CN-69/EXP2/03, this conference.

[11] SUTTROP, W. et al., paper IAEA-CN-69/EXP2/06, this conference.

[12] KARDAUN, O. J. W. F. et al., in *Plasma Physics and Controlled Nuclear Fusion Research 1992*, volume 3, pages 251–270, Vienna, 1993, IAEA.

[13] RYTER, F. et al., Plasma Phys. Controlled Fusion **40** (1998) 725.

[14] SUTTROP, W. et al., Physics and scaling of the H-Mode transition in ASDEX Upgrade, to be published in Plasma Phys. and Contr. Fusion.

[15] SUTTROP, W. et al., Plasma Phys. Controlled Fusion **39** (1997) 2051.

[16] GRUBER, O. et al., Plasma Phys. Controlled Fusion **39** (1997) B19.

[17] SUTTROP, W. et al., in *Proc. of the 1998 ICPP & 25th EPS Conference on Controlled Fusion and Plasma Physics, Praha, 1998)*, ECA volume 22A, pages 317–320, EPS, Petit-Lancy, 1998.

[18] LACKNER, K., Comments Plasma Phys. Controlled Fusion **15** (1994) 359.

[19] HERRMANN, W. et al., Plasma Phys. Controlled Fusion **40** (1998) 683.

[20] PEETERS, A. G. et al., Plasma Phys. Controlled Fusion **40** (1998) 703.

[21] HEIKKINEN, J. A. et al., Plasma Phys. Controlled Fusion **40** (1998) 693.

[22] ROGERS, B. N. et al., paper IAEA-CN-69/THP2/01, this conference.

[23] SCOTT, B. D. et al., paper IAEA-CN-69/TH1/05, this conference.

[24] SCOTT, B., Plasma Phys. Controlled Fusion **39** (1997) 471.

[25] NOTERDAEME, J.-M. et al., paper IAEA-CN-69/CDP/11, this conference.

[26] MERTENS, V. et al., Nucl. Fusion **37** (1997) 1607.

[27] MERTENS, V. et al., Plasma Phys. Controlled Fusion **36** (1994) 1307.

[28] BORRASS, K. et al., Contrib. Plasma Phys. **38** (1998) 130.

[29] GREENWALD, M. et al., Nucl. Fusion **28** (1988) 2199.

[30] SUTTROP, W. et al., Operational limits for high edge density H-Mode tokamak operation, to be published in Journ. Nucl. Mat.

[31] LANG, P. T. et al., Phys. Rev. Lett. **79** (1997) 1487.

[32] SUTTROP, W. et al., in *Europhysics Conference Abstracts (Proc. of the 24th EPS Conference on Controlled Fusion and Plasma Physics, Berchtesgaden, 1997)*, volume 21A, part IV, pages 1465–1468, Petit-Lancy, 1997, EPS.

[33] MARASCHEK, M. et al., in *Proc. of the 1998 ICPP & 25th EPS Conference on Controlled Fusion and Plasma Physics, Praha, 1998)*, ECA volume 22A, pages 492–495, EPS, Petit-Lancy, 1998.

[34] GUDE, A. et al., submitted to Nuclear Fusion (1998).

[35] GÜNTER, S. et al., paper IAEA-F1-CN-69/EX8/2, this conference.

[36] GÜNTER, S. et al., MHD Phenomena in Low and Reversed Shear Plasmas, submitted to Plasma Phys. Control. Fusion (1998).

[37] YU, Q. et al., Modelling of the neo-classical tearing mode and its stabilisation by ECCD/ECRH, to be published in Plasma Phys. and Contr. Fusion.

[38] ZOHM, H. et al., submitted to Phys. Rev. Lett. (1998).

[39] BURRELL, K. H. et al., Phys. Plasmas **4** (1997) 1499.

[40] SYNAKOWSKI, E. et al., Plasma Phys. Controlled Fusion **40** (1998) 581.

[41] WOLF, R. C. et al., paper IAEA-CN-69/EXP1/12, this conference.

[42] GUDE, A. et al., Plasma Phys. Controlled Fusion **40** (1998) 1057.